Journal of Materials Processing Tech. 255 (2018) 876–885

Contents lists available at ScienceDirect

Journal of Materials Processing Tech.

journal homepage: www.elsevier.com/locate/jmatprotec

Monitoring weld pool oscillation using reflected laser pattern in gas tungsten arc welding

Chunkai Li[a,b], Yu Shi[a,*], YuFen Gu[a], Peng Yuan[b]

[a] State Key Laboratory of Advanced Processing and Recycling Non-ferrous Metals, Lanzhou University of Technology, Lanzhou 730050, PR China
[b] Key Laboratory of Non-ferrous Metal Alloys and Processing, Ministry of Education, Lanzhou University of Technology, Lanzhou 730050, PR China

ARTICLE INFO

Keywords:
Weld pool oscillation
Single laser vision method
Image centroid
Weld penetration

ABSTRACT

A single laser vision method was proposed to carry out real-time sensing of the oscillation signal from the reflected laser pattern. A robust algorithm based on the image centroid of reflected laser pattern was developed to extract the oscillation frequency of weld pool and fluctuation amplitude of centroids of laser patternΔH_{cen}. The correlation between fluctuation amplitude of centroids of laser patternΔH_{cen} and oscillation amplitude of weld pool surface Δh_{act} were simulated based on the law of reflection. Several experiments were conducted in stationary and traveling welding processes with different penetration status. The oscillation frequency and ΔH_{cen} were extracted. An abrupt transition mode of oscillation frequency and Δh_{act} exists from partial to full penetration status in stationary welding process. By contrast, an abrupt transition occurs in Δh_{act} in the case of traveling welding process. Two transition modes of oscillation frequency, continuous and abrupt change mode, occurred with different welding speeds, which correlated with the oscillation behavior of weld pool surface.

1. Introduction

In recent years, trends in high productivity and high-quality welding leaned toward process automation, which has stimulated the increased use of automation and associated systems. As one of the major arc welding processes, gas tungsten arc welding (GTAW) has been widely used in the production of high-quality components for reactor pressure vessels and aerospace structures due to its high weld quality and easy automation. Incomplete penetration is the main and long-standing issues affecting the weld quality in automatic GTAW welding process. Manual GTAW is still applied in many situations to obtain consistent and complete penetration. Hence, sensing and controlling weld penetration in the GTAW welding process have been key issues to developing next-generation intelligent automatic weld machines.

Numerous works were conducted to find the feature signal that can be used to sense and control weld penetration in GTAW welding process, such as infrared temperature, machine vision, X-ray, and weld pool oscillation. The temperature distribution of weld pool is believed to provide valuable information on the penetration status because welding is essentially a thermal process. Chen and Chin (Chen and Chin, 1990) developed an infrared camera to monitor the temperature distribution surrounding the molten pool and found that an exponential relationship exists between the penetration depth and temperature profile. Vasudevan et al. (Vasudevan et al., 2011) measured temperature profile of weld pool using IR camera and computed temperature gradient of macroscopic temperature gradient during GTAW welding process. They found that an inverse linear relationship exists between temperature gradient and penetration depth. Unfortunately, the strong radiation of arc and tungsten electrode have made it very difficult, if not impossible, to measure the actual temperature distribution of molten pool, which contains direct and exact information on penetration status. A skilled welder can estimate the weld penetration by observing pool surface, which indicated that sufficient information on penetration must be contained in the pool surface. Based on the experience of a skilled welder, many researchers have attempted to use machine vision monitor and control weld penetration. Liu et al. (Liu et al., 2015) extracted the boundary of weld pool surface from the passive vision images by using active contour method. Wu and Chen (Wu and Chen, 2007) proposed a passive visual sensing system to measure the weld shape parameters and a neural network models based on 2D features of the weld pool was built to control weld penetration during aluminum alloy GTAW. Obtaining accurate three-dimension (3D) information on pool surface from machine vision sensor is a challenging task due to the arc interference and specular peculiarity of pool surface. Zhang and his co-workers (Song and Zhang, 2008; Zhang et al., 2012, Zhang et al., 2006) in University of Kentucky firstly proposed a laser vision method to real-time monitor and reconstruct the three-dimension (3D) weld pool surface by multiline or dot matrix-laser

* Corresponding author.
E-mail address: shiyu@lut.cn (Y. Shi).

https://doi.org/10.1016/j.jmatprotec.2018.01.037
Received 4 December 2017; Received in revised form 24 January 2018; Accepted 25 January 2018
Available online 31 January 2018
0924-0136/

illuminating and reflecting imaging. Using this method, Liu and Zhang (Liu et al., 2013; Liu and Zhang, 2015) built an ANFIS model to estimate the correlation between 3D weld pool surface with skilled human welder's response and control penetration in pipe GTAW process. However, the algorithm of 3D reconstruction pool surface is relatively complicated and time consuming. The correlation between top geometry of weld pool and penetration status of bottom pool is indirect and empirical, which requires further investigation.

Among the feature signals that can be used to characterize the penetration status, weld pool oscillation could provide a direct information correlation with weld penetration. This sensing method is based on the phenomenon that oscillation frequency of weld pool is related to the weld pool geometry, volume, and mass of molten metal when excited by external force, which has direct mathematical relationship with penetration status (Xiao and Den Ouden, 1990; YOO and Richardson, 1993). Two traditional methods were proposed to monitor the oscillation frequency of weld pool surface: arc voltage and arc radiation. Xiao and Den Ouden (Xiao and Den Ouden, 1990) built an arc voltage sensing system to monitor the oscillation frequency of weld pool in stationary welding condition and found that the oscillation frequency in partial penetration is evidently larger than that in full penetration. YOO and Richardson (YOO and Richardson, 1993) proposed an arc voltage and radiation synchronous sensing system to detect the oscillation signal from the arc radiation and voltage. They found that arc radiation is more sensitive to oscillation signal than arc voltage, and an abrupt transition exists for oscillation frequency from partial to full penetration in stationary and low welding speed. The significant drawback for the two methods is that they can only be used in limited welding conditions, such as stationary, step or low speed, short arc length, and only the one-dimension oscillation signal can be detected. Other oscillation behavior, such as oscillation amplitude of pool surface and oscillation direction, may also be correlated with penetration status and require further study. Sensing high quality and full-dimensional oscillation signal from pool surface remains to be the major difficulty for weld pool oscillation method.

Along this direction, many researchers made attempt to monitor the pool oscillation using three-dimension laser vision method recently. Zhang et al (Zhang et al., 2017) observed and analyzed the stationary pool oscillation in three dimensions using dot-matrix laser vision method and found that three oscillation mode exists in different penetration status. In our previous work, Shi and his co-workers (Shi et al., 2015) monitored the oscillation frequency using multiline laser vision method and three kinds of characteristics frequency of pool surface were found from partial to full penetration in low welding speed. However, the image processing algorithm used to extract oscillation frequency needs to calibrate the original image firstly and compute the entire brightness value of each image, which is very complex and time consuming. 3D oscillation signal, such as oscillation amplitude of weld pool surface, cannot be detected due to the ambiguous correlation between the dynamic evolution of weld pool surface and brightness value of each image. The effect of welding speed on oscillation frequency and oscillation amplitude of pool surface also did not investigated. To overcome the disadvantage of complex image processing algorithm and one-dimension oscillation signal of weld pool, a single laser vision method and an algorithm based on the image centroid of each image were proposed. Then, the correlation between the fluctuation amplitude of centroids in the image ΔH_{cen} and oscillation amplitude of weld pool surface Δh_{act} was simulated based on the law of reflection. Finally, the oscillation frequency and amplitude of weld pool surface Δh_{act} for stationary and traveling welding process with different penetration status were analyzed.

2. Sensing system

The sensing system is shown in Fig. 1. A 500 mW illumination laser with a wavelength of 669.5 nm generates a single-line pattern which is projected onto the pool surface behind the electrode. The laser generator is placed onto an OYZ plane at 30° and 40 mm away from weld torch. An imaging plane with dimensions of $60 \times 60mm$ was placed 50 mm away from the welding torch, which was used to intercept the reflected laser pattern. A high-speed CCD camera was used to sense reflected laser pattern on the imaging plane. The sample frequency of the camera is set to 800 Hz. Pulsed GTAW welding method was applied to trigger the weld pool surface into oscillation.

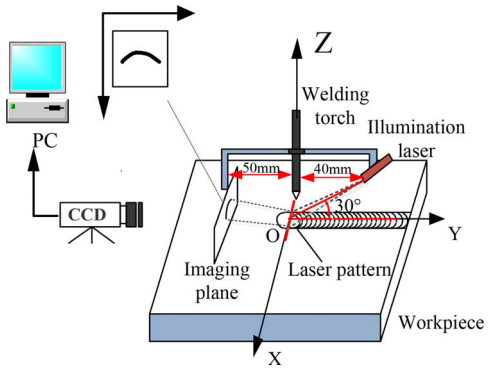

Fig. 1. Sensing system.

3. Principle of measurement

In peak current period, the weld pool surface is triggered and depressed by the high plasma jet. In base current period, the weld pool surface is oscillated due to the broke balance among the surface tension, gravity, and plasma jet. Under the action of surface tension of molten metal, the weld pool surface tends to move toward the equilibrium position and cause weld pool oscillation. Owing to the specular property of pool surface, the reflected laser patterns can synchronously deform with the surface oscillation of weld pool. Although the displacement of weld pool surface in different states (states 1, 2, 3) is very weak shown in Fig. 2, the reflected angle variation and displacement of laser pattern on the imaging plane are evident. The amplitude oscillation of weld pool surface can be calculated from the displacement of laser pattern based on the law of optical reflection.

4. Algorithm to extract oscillation signal

Typical reflected laser pattern images captured by high-speed camera during welding process are shown in Fig. 3. The reflected laser pattern is deformed with the oscillation of pool surface and the variation of centroids of reflected laser pattern is greatly and periodically, which marked with a red circle.

Utilizing the variation of centroids of reflected laser pattern, a robust algorithm was developed to extract the oscillation signal from images. Fig. 4 shows the flow chart of the algorithm. This algorithm mainly consists of two sections: image preprocessing and extraction centroid. In the image preprocessing section, the original image was processed by selecting the ROI image, automatic thresholding binarization technology and the reflected laser pattern segment was separated from background shown in Fig. 5. In extraction centroid section, the position of centroids of laser pattern in the image was calculated by the following equation:

$$\begin{cases} x_0 = \dfrac{\sum_{x=1}^{m}\sum_{y=1}^{n} f(x,y)\times x}{\sum_{x=1}^{m}\sum_{y=1}^{n} f(x,y)} \\ y_0 = \dfrac{\sum_{x=1}^{m}\sum_{y=1}^{n} f(x,y)\times y}{\sum_{x=1}^{m}\sum_{y=1}^{n} f(x,y)} \end{cases} \tag{1}$$

Where x_0 and y_0 represent the coordinates of centroids of laser pattern; m and n represent the size of pixels in the x and y direction, respectively.

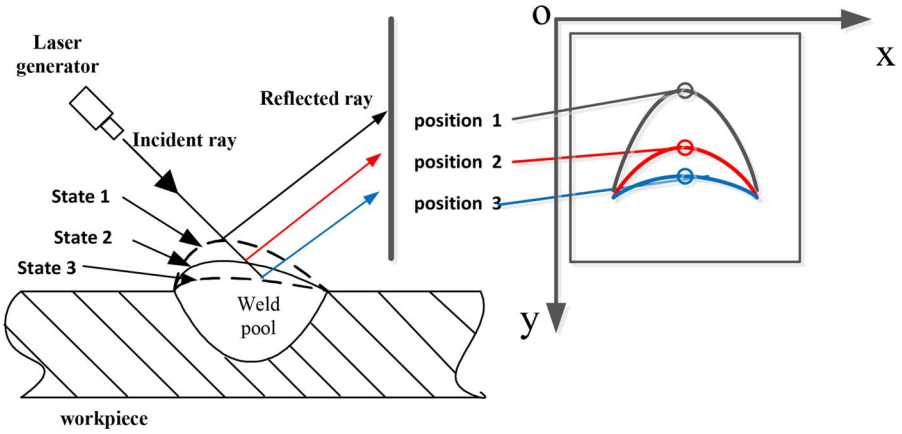

Fig. 2. Principle of measurement.

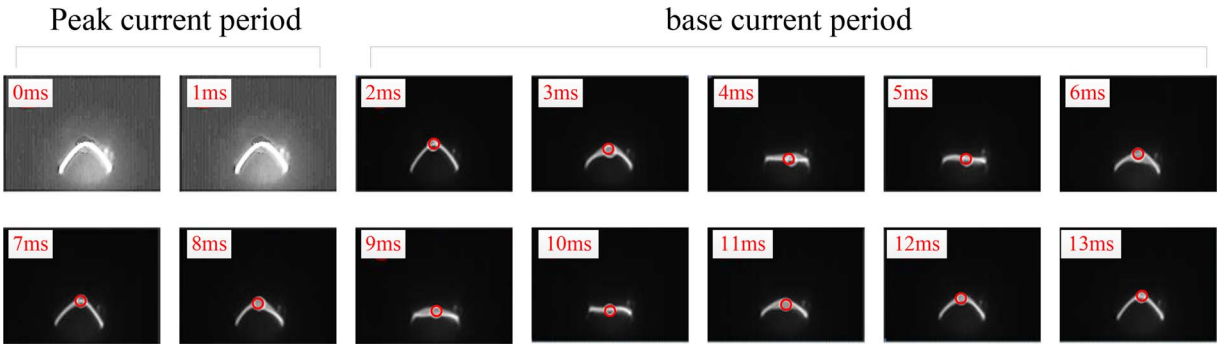

Fig. 3. Typical reflected laser pattern in one oscillation period.
(I_p = 144 A, I_b = 70 A, duty rate = 44%, pulse frequency = 3.5 Hz, sample frequency = 800 Hz, V = 1.3 mm/s).

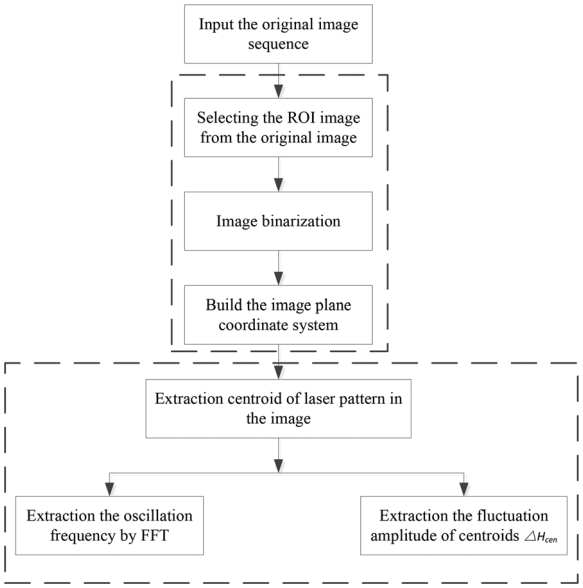

Fig. 4. Flow chart of the algorithm.

Fig. 5. Image preprocessing. (a) Original image. (b) ROI image. (c) Binarized image.

Fig. 6(a) shows the variation of coordinates of centroid of laser pattern in continuous 300 images extracted by the centroid algorithm. The variation of coordinates in the y-direction is found to be apparent and periodic, whereas the change in the x-direction is very weak and irregular. The variation of coordinates of centroids of laser pattern in y direction was chosen as the oscillation signal. The fast Fourier transform (FFT), which is calculated by the following equation, was utilized to extract the oscillation frequency from the time domain.

$$X(n) = \sum_{n=0}^{N-1} x(n) e^{-j\frac{2\pi}{N}n}. \tag{2}$$

Fig. 6(b) shows the frequency domain signal transformed by FFT and the characteristic frequency is approximately 135.6 Hz, which nearly agrees with the manual count of the framed laser images.

The fluctuation amplitude of centroids in the image (in pixel) ΔH_{cen} during pool oscillation (base current period) was calculated by the following equation:

$$\Delta H_{cen} = H_{cen-\max} - H_{cen-\min}. \tag{3}$$

Where$H_{cen-\max}$ and $H_{cen-\min}$ represent the maximum and minimum of coordinate of centroids in y direction, respectively. Based on the Eq. (3), the ΔH_{cen} in Fig. 3 is about 79 pixels.

Compared with the brightness value of the image-processing algorithm proposed in our previous work (Shi et al., 2016), this algorithm neither requires the calibration of original image nor needs the calculation of the entire image brightness value. This algorithm extracts the coordinates of laser pattern centroids with only 8 ms under the condition of existing hardware, which is significantly less than the brightness value image-processing algorithm (28 ms) and sufficiently satisfies the real-time sensing demands.

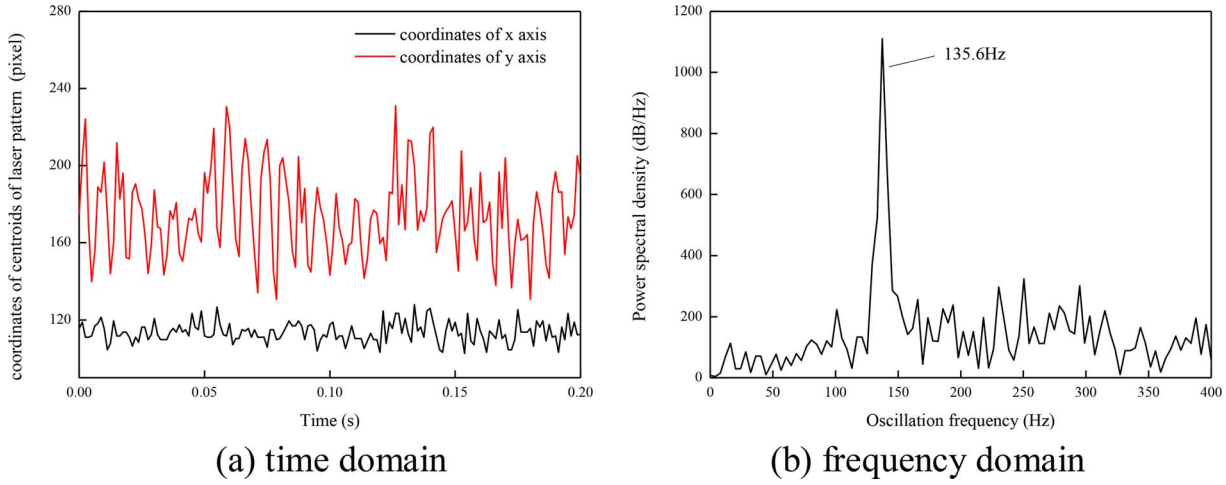

Fig. 6. Oscillation signal extracted by centroid algorithm. (a) Time domain. (b) Frequency domain.

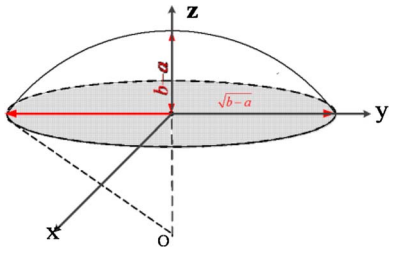

Fig. 7. Model of weld pool surface.

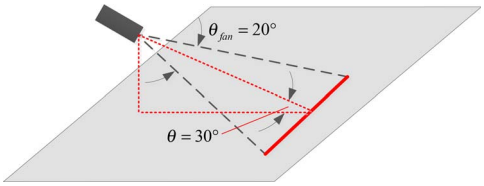

Fig. 8. Definition of fan angle and laser-level angle.

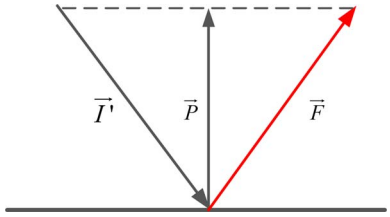

Fig. 10. Model of incident rays reflected by weld pool surface.

Fig. 9. Mathematical relationship among $\overrightarrow{I_{1,i}'}$, $\overrightarrow{p_{1,i}}$, and $\overrightarrow{F_{1,i}}$.

5. Simulation of reflection from pool surface

Oscillation amplitude of pool surface Δh_{act} is one of the important characteristics of oscillation behavior in GTAW, which has a direct relationship with the oscillation mode and penetration depth. Owing to the existence of a direct mathematical relationship between displacement of pool surface and centroid of laser pattern, the fluctuation amplitude of centroids of laser pattern in the image ΔH_{cen} can be used to represent the amplitude of weld pool surfaceΔh_{act}. A simulation based on the law of optical reflection is carried out to quantify the relationship between the variations of height amplitude of weld pool surface and coordinates of laser pattern centroids.

5.1. Modeling

The weld pool surface is simulated using part of a sphere shown in Fig. 7 and expressed by the following equation:

$$F(x, y, z) = \begin{cases} x^2 + y^2 + (z + a)^2 - b^2 = 0 \\ z >= 0 \end{cases}, \tag{4}$$

where a, b is coordinate of the sphere center in the space coordinate system, $b - a$ is the height of weld pool, and $\sqrt{b^2 - a^2}$ is the radius of weld pool, which is shown in Fig. 7.

The continuous single-line laser is replaced using assumed 1×30 dot matrix. The expression of 1×30 dot matrix in space coordinate system can be expressed by the following equation:

$$\begin{cases} x_i = x_0 + (\tan(\theta_{fan} i)) \bullet n \\ y_i = y_0 + (y0 - \frac{z0}{\tan\theta}) \bullet n \\ z_i = z_0 + z_0 \bullet n \end{cases}, \tag{5}$$

where θ_{fan} is the fan angle of projected single-line pattern; θ is the angle of laser generator between A horizontal plane, which is shown in Fig. 8. $[x_0, y_0, z_0]$ is the coordinate of laser generator in space coordinate

Table 1
Simulation parameters.

Simulation No	Coordinate of illumination laser	θ_{fan}/°	θ/°	L/mm	A/mm	B/mm	Weld width/mm	Height of weld pool/mm
1	(0,43,25)	20	30	50	60	60	4.25	0.1
2	(0,43,25)	20	30	50	60	60	4.25	0.2

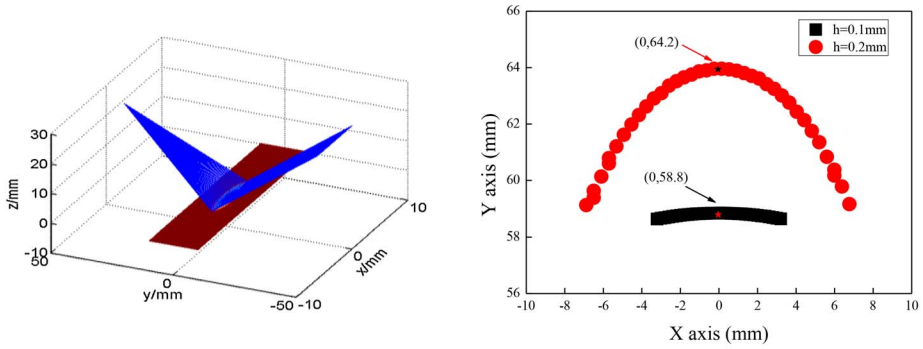

(a) Simulation of weld pool surface with incident laser (b) Calculated reflected laser pattern on the imaging plane

Fig. 11. Simulation results. (a) Simulation of weld pool surface with incident laser. (b) Calculated reflected laser pattern on the imaging plane.

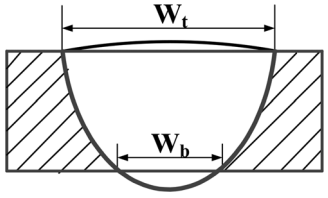

Fig. 12. Schematic of weld pool geometry.

Table 2
Welding parameters.

No	Peak current/ A	Base current/ A	Duty ratio/ %	Pulse frequency/ Hz	Average current/ A	Welding speed/ (mm/s)	Arc time/s
1	144	70	44%	3.5	102.56	0	3–20 s
2	144	70	44%	3.5	102.56	1.5–0.4	–
3	220	70	54%	3.5	151	3.1–2.1	–

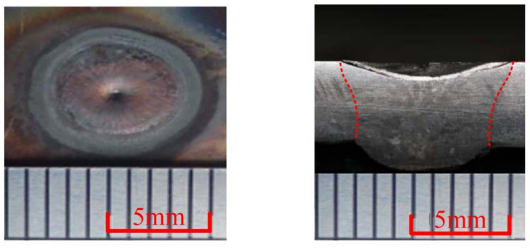

(a) weld bead shape (b) cross-sectional shape

Fig. 14. Typical weld bead in full penetration (Experiment No 1; arc time 16 s). (a) Weld bead shape. (b) Cross-sectional shape.

system; $\overrightarrow{l_{1,i}} = [\tan(\theta_{fan} i), y0 - \frac{z0}{\tan(\theta)}, z0]$ and $\overrightarrow{l_{1,i}'} = \frac{\vec{l}}{\sqrt{(\tan(0.77i))^2 + (y0 - \frac{z0}{\tan(\theta)})^2 + Z0^2}}$ are direction and unit vectors of the projected single-line, respectively.

The imaging plane in the space coordinate system is expressed by the following equation:

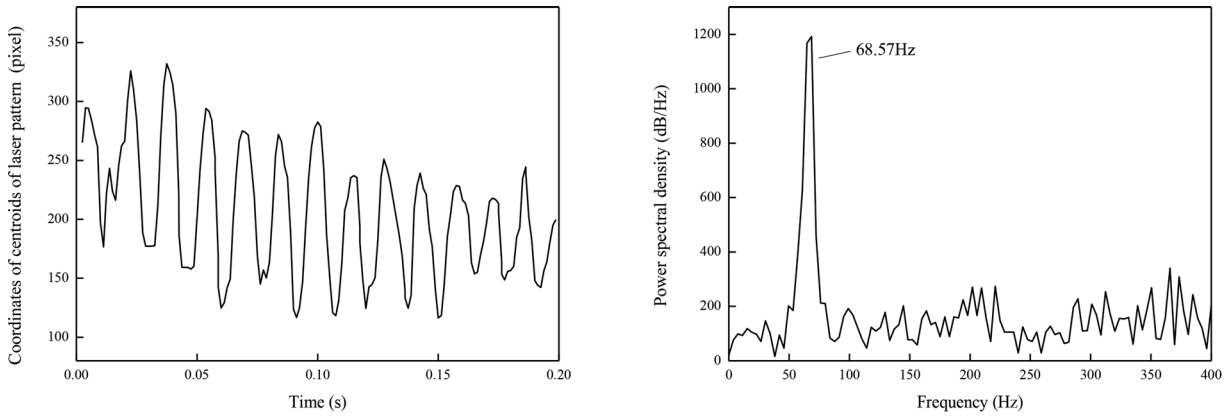

(a) time domain (b) frequency domain

Fig. 13. Typical oscillation signal in full penetration (Experiment No 1; arc time 16 s). (a) Time domain. (b) Frequency domain.

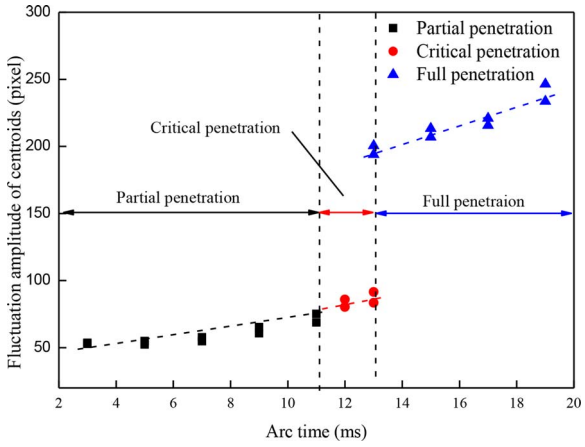

Fig. 15. Fluctuation amplitude of centroidsΔH_{cen} with arc time t.

$$\begin{cases} y = -L \\ -\frac{A}{2} \le x \le \frac{A}{2}, \\ 0 \le z \le B \end{cases} \tag{6}$$

where L is the distance between weld torch and imaging plane; A and B is the length and width of imaging plane, respectively.

5.2. Simulation algorithm

First, combining Eqs. (4) and (5), the coordinates of incident point on the pool surface$s_i = [x_i', y_i', z_i']$can be calculated, and the unit surface normal vector $\overrightarrow{p_{1,i}}$ at pint s_i can be expressed as

$$\overrightarrow{p_{1,i}} = \frac{\left(\frac{\partial F(x,y,z)}{\partial x}, \frac{\partial F(x,y,z)}{\partial y}, \frac{\partial F(x,y,z)}{\partial z}\right)}{\sqrt{\left(\frac{\partial F(x,y,z)}{\partial x}\right)^2 + \left(\frac{\partial F(x,y,z)}{\partial y}\right)^2 + \left(\frac{\partial F(x,y,z)}{\partial z}\right)^2}}. \tag{7}$$

Second, based on the law of specular reflection, a mathematical relation exists among the $\overrightarrow{I'}$(unit vector of projected ray), $\overrightarrow{p_{1,i}}$(unit surface normal vector $\overrightarrow{p_{1,i}}$ at pointss_i), and $\overrightarrow{F_{1,i}}$(unit vector of reflected ray), as shown in Fig. 9. $\overrightarrow{F_{1,i}} = [P''x_i, p''y_i, p''z_i]$ can be calculated by the following equation:

$$\overrightarrow{I_{1,i}'} + 2\overrightarrow{P_{1,i}} = \overrightarrow{F_{1,i}} \tag{8}$$

Then, the reflected laser can be expressed by

$$\begin{cases} x''_i = x'_i + p''x_i \bullet n \\ y''_i = y'_i + p''y_i \bullet n \\ z''_i = z'_i + p''z_i \bullet n \end{cases} \tag{9}$$

Third, combining Eqs. (9) and (6), the corresponding reflected laser dots on the imaging plane can be calculated. Fig. 10 shows the modeling of incident rays reflected by the weld pool surface.

5.3. Simulation results

The reflected laser pattern on the image with different height of pool surface was simulated, and the simulation parameters are shown in Table 1.

Fig. 11(a) shows the simulation of weld pool surface with reflected laser pattern. Fig. 11(b) shows the simulated laser pattern on the imaging plane, which is similar to the laser pattern captured by high-speed camera, as shown in Fig. 3. The coordinates of laser pattern centroids in the imaging plane with simulation No 1 and 2 are (0, 64.2) and (0, 58.8), i.e. the variation of centroids in the y-direction is 5.1 mm. The actual variation of centroids in an image is approximately is 40.8 *pixel* because the ratio of pixel size in an image to millimeter size in an imaging plane is approximately 9.0, i.e. $1mm = 9pixel$. The small amplitude oscillation (0.1 mm) of pool surface can be considerably amplified by the laser pattern centroids (40.8 pixels) in the image, and the magnification is approximately 408. By quantifying the relation between centroids variation in the image and height variation in the weld pool, the fluctuation amplitude of centroids of reflected laser pattern ΔH_{cen} can be used to represent the oscillation amplitude of weld pool surfaceΔh_{act}.

6. Experimental produce

Generally, three types of penetration status are available in GTAW weld pool, partial penetration, critical penetration, and full penetration, which defined by the ratio of bottom and top width of weld pool, as shown in Fig. 12. In critical penetration, W_b/W_t is less than 0.4. In full penetration, W_b/W_t is larger than 0.4.

The experiments aimed to study the characteristics of oscillation frequency and oscillation amplitude of pool surface in different penetration depth under stationary and traveling arc welding process. The 304 stainless steel with 3 mm thickness was used as workpiece. A standard 2% thoriated tungsten electrode which is 2.4 mm in diameter was used as a cathode. The arc length and flow rate of argon shielding gas are 3 mm and 8 L/min, respectively. The welding parameters are shown in Table 2. Experiment 1 was designed in stationary welding

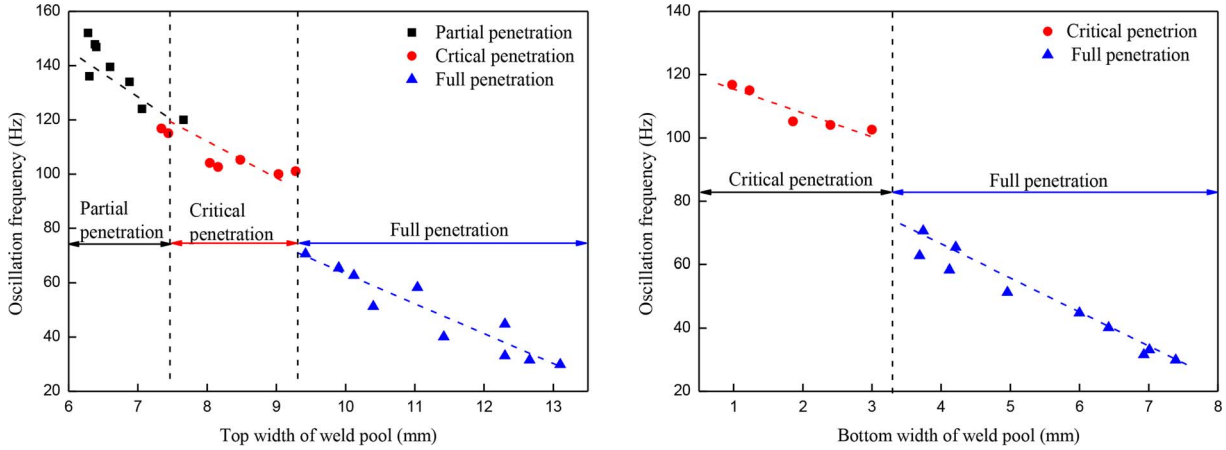

(a) top width of weld pool (b) bottom width of weld pool

Fig. 16. Variation of oscillation frequency with weld width in stationary welding. (a) Top width of weld pool. (b) Bottom width of weld pool.

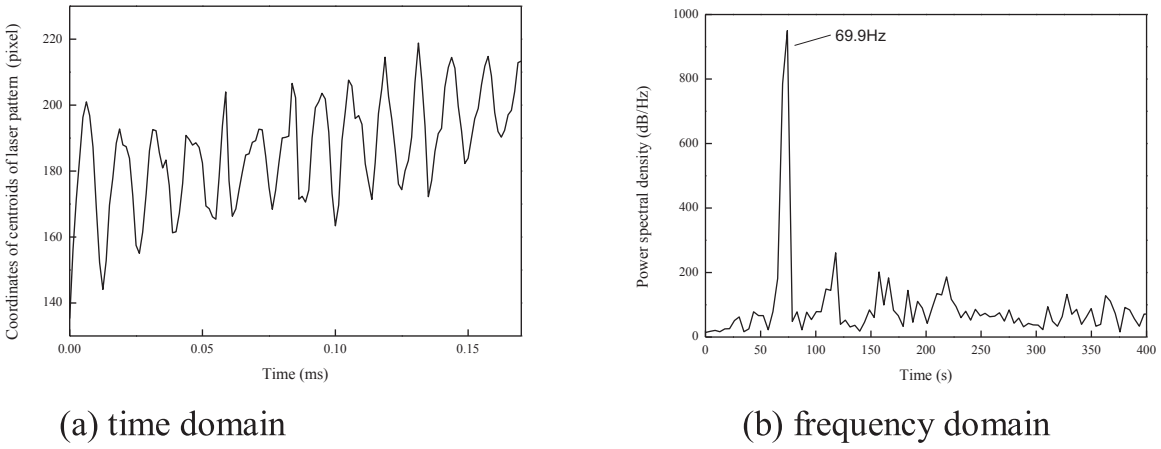

Fig. 17. Typical oscillation signal in partial penetration (Experiment No 3; welding speed 2.8 mm/s). (a) Time domain. (b) Frequency domain.

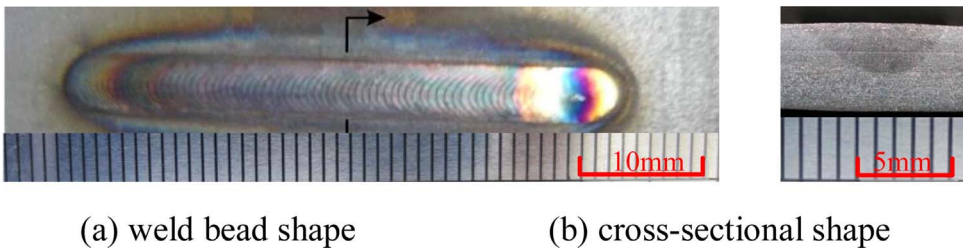

Fig. 18. Typical weld bead and its cross-sectional shape in partial penetration (Experiment No 3; welding speed 2.8 mm/s). (a) Weld bead shape. (b) Cross-sectional shape.

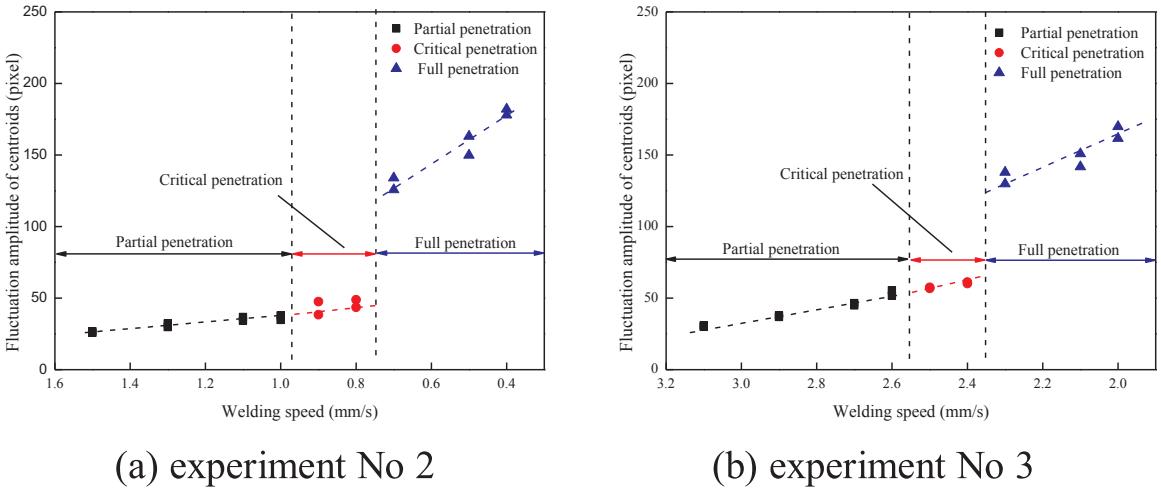

Fig. 19. Fluctuation amplitude of centroidsΔH_{cen} with welding speed. (a) Experiment No 2. (b) Experiment No 3.

process, and different weld penetration were obtained by the change in arc time. Experiments 2 and 3 were designed in traveling welding process, and different weld penetration were obtained by welding speed variation.

7. Experimental results and discussion

7.1. Stationary arc welding experiment

Numerous partial, critical, and full penetration in stationary welding condition were obtained, and the oscillation frequency and ΔH_{cen} were synchronously measured. Figs. 13 and 14 show the typical oscillation signal and weld bead in full penetration under stationary welding process, respectively. Fig. 15 shows the variation of ΔH_{cen} with arc time t. The ΔH_{cen} increased with arc time$t$ and an abrupt transition occurred in a critical arc time point t_c(approximately 12 s), in which penetration status transferred from critical to full penetration. Considering the relationship between fluctuation amplitude of centroids ΔH_{cen} and oscillation amplitude of weld pool surface Δh_{act} discussed in Section 5, an abrupt transition must also be occurred inΔh_{act}. Fig. 16(a) and (b) shows the variation of oscillation frequency with top width W_t and bottom width W_b of weld pool, respectively. In the case of partial and critical penetration, the oscillation frequency continuously varies, i.e. no abrupt transition occurred in oscillation frequency. In the case of full penetration, an abrupt transition occurred in oscillation frequency.

7.2. Traveling arc welding

Through experimental results in Section 7.1, an abrupt transition both occurred in Δh_{act} and oscillation frequency from partial to full penetration in stationary welding process. Further investigating whether the variation of oscillation frequency and Δh_{act} in traveling welding process has a similar behavior is necessary. Traveling speed is

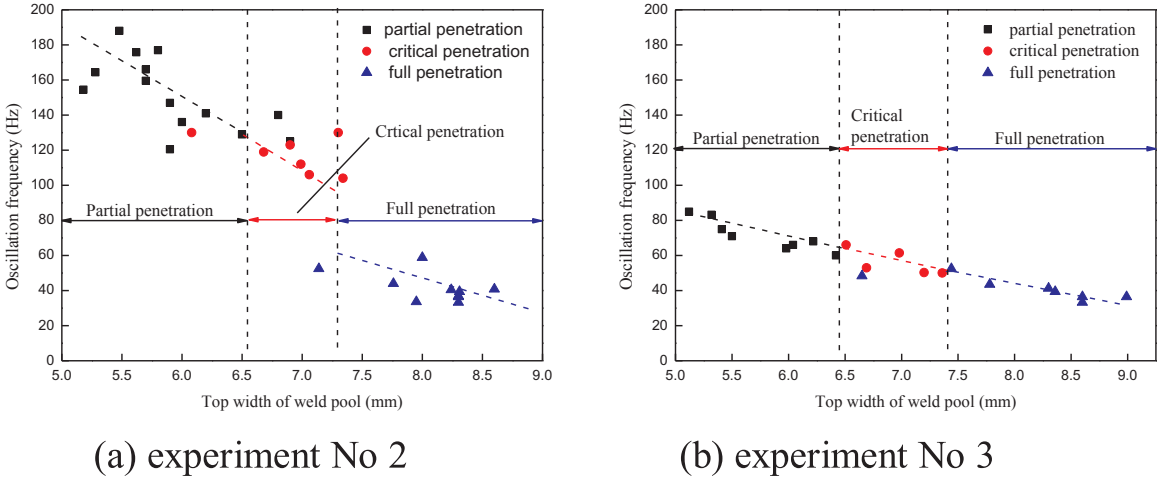

Fig. 20. Variation of oscillation frequency with top width of weld pool. (a) Experiment No 2. (b) Experiment No 3.

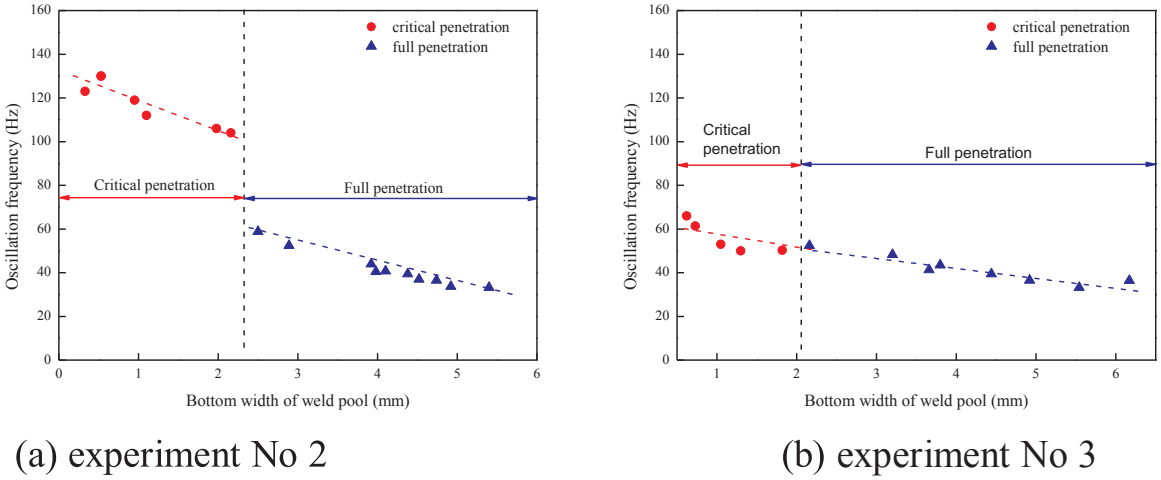

Fig. 21. Variation of oscillation frequency with bottom width of weld pool. (a) Experiment No 2. (b) Experiment No 3.

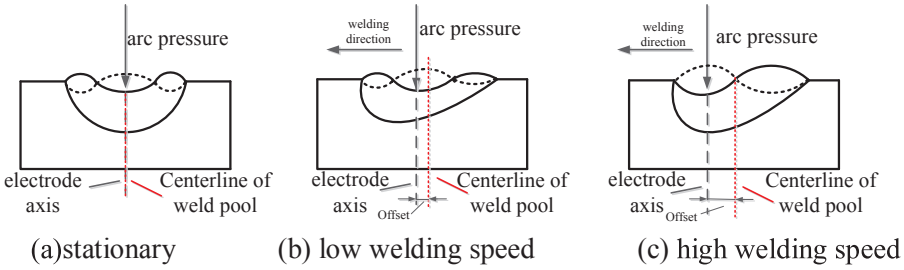

Fig. 22. Oscillation mode with different welding speeds. (a) Stationary. (b) Low welding speed. (c) High welding speed.

the dominant factor that affects the quality of oscillation signal for traditional sensing methods. Two groups of experiment with different traveling speeds were conducted to study the effect of traveling speed on characteristics of oscillation frequency, Δh_{act}, and sensing quality for single laser vision method.

Figs. 17 and 18 are typical oscillation signal and weld bead in partial penetration with a traveling speed of 2.8 mm/s (experiment No 3), respectively. Fig. 17(a) shows the oscillation signal in time domain, which exhibits strong periodic. The traveling speed slightly affects sensing quality of weld pool oscillation for single laser vision method. This method has higher adaptability to welding speed compared to that of the traditional method. Fig. 19(a) and (b) shows the variation of ΔH_{cen} with welding speed in experiment No 2 and 3, respectively. The ΔH_{cen} increased with decreasing welding speed and an abrupt transition occurred in the transition from critical to full penetration status, which is similar to the stationary welding process. The ΔH_{cen} in experiment No 2 is evidently less than stationary welding process with partial and full penetration, which indicates that traveling speed has a considerable effect on the oscillation amplitude of weld pool surfaceΔh_{act}. Figs. 20 and 21 show the variation of oscillation frequency with top and bottom widths of weld pool, respectively. Unlike the stationary welding process, two variation modes of oscillation frequency appeared. In experiment No 2 with low welding speed, an abrupt mode of oscillation frequency occurred from partial to full penetration. A continuous mode of oscillation frequency occurred from partial to full penetration with high welding speed (experiment No 3). From the preceding experiment results, the oscillation behavior of weld pool in traveling welding process is complex and requires further analysis.

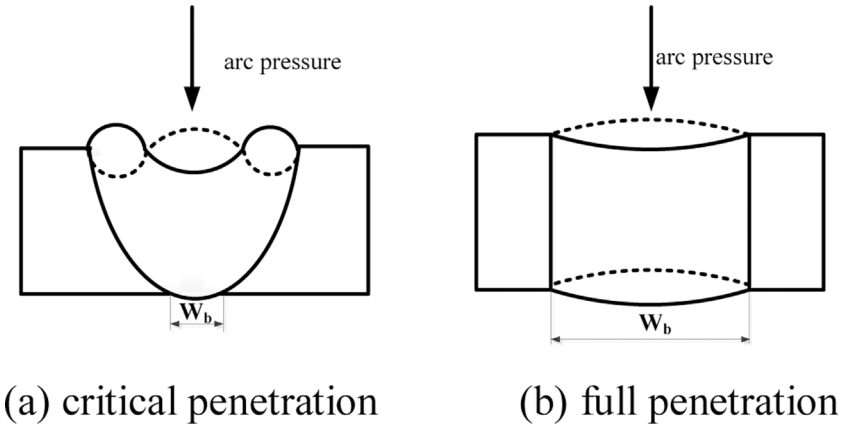

Fig. 23. Stationary and low welding speed welding process. (a) Critical penetration. (b) Full penetration.

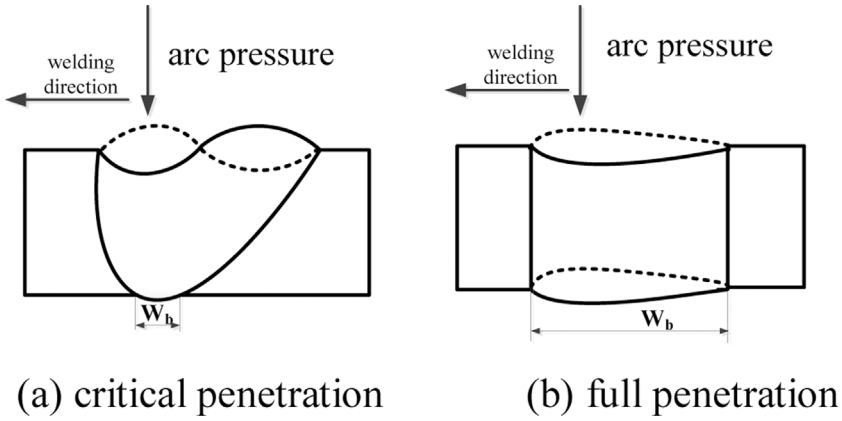

Fig. 24. High welding speed welding process. (a) Critical penetration. (b) Full penetration.

7.3. Discussion

To explain the experiment results described in Section 7.1 and 7.2, conducting a detailed analysis of the oscillation behavior of partial, critical, and full penetration is necessary.

7.3.1. Partial penetration

In stationary welding process, the arc is located exactly in the center of weld pool. The electrode axis is coincident with the weld pool centerline, as shown in Fig. 22(a). Under this condition, the weld pool surface is symmetrically depressed in peak current, and the molten metal in the weld pool is pushed toward the radial direction. The oscillation behavior of weld pool in base current period is symmetrical during base current, as shown in Fig. 22(a) (experiment No 1). In traveling weld process, the weld pool is gradually elongated and the electrode axis shifts from the weld pool centerline toward the front edge of the weld pool. A large welding speed V leads to a large offset S between the electrode axis and weld pool centerline. Owing to the relatively low welding speed (experiment No 2), the offset S is relatively small and the molten metal in the weld pool is predominantly pushed to the radial direction in peak current period. The oscillation behavior of weld pool surface nearly remains in symmetrical mode, as shown in Fig. 22(b). With relatively high welding speed V or large offset S(experiment 3), the molten metal in the weld pool is easily pushed to the rear part of the weld pool, which resulted in an evident asymmetrical shape of weld pool. During base current period, the weld pool surface is oscillated in asymmetrical mode, as shown in Fig. 22(c). In the case of partial penetration, the molten metal in the weld pool is backed by the solid metal, and the oscillation behavior can be assumed as a free surface wave. Xiao and Den Ouden (Xiao and Den Ouden, 1993) proposed a model to analyze the oscillation frequency for symmetrical and asymmetrical modes of partial penetration. They found that the oscillation frequency of weld pool in symmetrical mode is evidently higher than that of the asymmetrical mode in partial penetration, which agrees with the present experiment results in Section 7.2. The occurrence of a continuous oscillation frequency mode in experiment No 3 is caused by asymmetrical oscillation of weld pool surface.

7.3.2. Critical penetration and full penetration

In case of critical and full penetration, the solid metal in the backside of workpiece is melted into a molten state. The occurrence of molten metal in the backside of weld pool may influence the oscillation behavior due to the generation of a new extra free surface and degrees of freedom. In case of critical penetration with relatively smallW_b, most of the molten metal is still supported by the solid metal. The oscillation behavior is kept consistent with the partial penetration, as shown in Figs. 23(a) and Fig. 24(a). After realizing full penetration, i.e., W_b is relatively large, the solid metal in the bottom of workpiece disappears, and the molten metal is only supported by the surface tension of the bottom pool. The oscillation behavior in this condition can be assumed as a stretched membrane, as shown in Figs. 23(b) and Fig. 24(b). Zacksenhouse and Hardt (Zacksenhouse and Hardt, 1983) built an analytical model based on the theory of stretched membrane to study the oscillation frequency in stationary full penetration pool. They found that in stationary full penetration pool the oscillation frequency is obviously lower than partial penetration, which is consist with our experiment results in Sections 7.1 and 7.2. Owing to the absence of solid boundary constraint at the bottom in this mode, the oscillation amplitude of weld pool Δh_{act} must be more intense than partial and critical penetration, which is also verified by the present experiment results in Sections 7.1 and 7.2.

The oscillation behavior of weld pool surface in traveling welding process is considerably more complex than in stationary welding process. The occurrence of an abrupt transition in Δh_{act} and oscillation

frequency from partial to full penetration can be used to real-time monitor and control weld penetration in GTAW welding process.

8. Conclusions

Oscillation frequency and amplitude of weld pool surface for stationary and traveling welding process with different penetration status were characterized and analyzed from the centroid variation of reflected laser pattern in the image. Through the preceding experiments, the following conclusions can be obtained in this work.

(1) A single laser vision system was proposed to real-time monitor the oscillation frequency and amplitude of weld pool surface Δh_{act} in GTAW welding process. A robust algorithm, based on the centroid of reflected laser pattern in the image, is proposed to extract the oscillation frequency and fluctuation amplitude of centroids of reflected laser patternΔH_{cen}.
(2) The correlation between the centroid coordinate variation of reflected laser pattern ΔH_{cen} and oscillation amplitude of weld pool Δh_{act} was simulated based on the spherical mirror assumption of pool surface. The small amplitude oscillation of weld pool surface Δh_{act} can be considerably amplified by the centroids of laser pattern in the imageΔH_{cen}.
(3) In the case of stationary welding process, an abrupt transition both occurred in the oscillation frequency and amplitude of weld pool surface Δh_{act} from partial to full penetration.
(4) In the case of traveling welding process, an abrupt transition also exists in the oscillation amplitude of weld pool surfaceΔh_{act}. Two transition modes of oscillation frequency, continuous and abrupt change modes, occurred with different welding speeds, which correlated with the oscillation behavior weld pool surface.
(5) The abrupt transition in oscillation frequency and amplitude of weld pool surface Δh_{act} from partial to full penetration can be used to monitor and control the penetration in real-time.

Acknowledgments

This work was supported by National Natural Science Foundation of China (#51765037), Plan for Basic Research Creative Group of Gansu Province (#17JR5RA107), Project for Collaborative Innovation Team of Universities in Gansu Province (#2017C-07) and Outstanding Students Overseas Exchange Foundation of Lanzhou University of Technology of China.

References

Chen, W., Chin, B., 1990. Monitoring joint penetration using infrared sensing techniques. Weld. J. 69, 181–185.
Liu, J., Fan, Z., Olsen, S.I., Christensen, K.H., Kristensen, J.K., 2015. Boosting active contours for weld Pool visual tracking in automatic arc welding. IEEE Trans. Autom. Sci. Eng. 14 (12), 1096–1108.
Liu, Y., Zhang, W., Zhang, Y., 2013. ANFIS modeling of human welder's response to three-dimensional weld pool surface in GTAW. J. Manuf. Sci. Eng. 135, 021010.
Liu, Y., Zhang, Y., 2015. Iterative local ANFIS-based human welder intelligence modeling and control in pipe GTAW process: a data-driven approach. IEEE/ASME Trans. Mechatron. 20, 1079–1088.
Shi, Y., Li, C., Du, L., Gu, Y., Zhu, M., 2016. Frequency characteristics of weld pool oscillation in pulsed gas tungsten arc welding. J. Manuf. Process. 24, 145–151.
Shi, Y., Zhang, G., Ma, X., Gu, Y., Huang, J., Fan, D., 2015. Laser-vision-based measurement and analysis of weld pool oscillation frequency in GTAW-P. Weld. J. 94, 176–187.
Song, H.S., Zhang, Y.M., 2008. Measurement and analysis of three-dimensional specular gas tungsten arc weld pool surface. Weld. J. 87, 85–95.
Vasudevan, M., Chandrasekhar, N., Maduraimuthu, V., Bhaduri, A., Raj, B., 2011. Real-time monitoring of weld pool during GTAW using infra-red thermography and analysis of infra-red thermal images. Weld. World 55, 83–89.
Wu, J., Chen, S., 2007. Software system designs of real-time image processing of weld pool dynamic characteristics, robotic welding. Intelligence and Automation. Springer, pp. 303–309.
Xiao, Y., Den Ouden, G., 1990. A study of GTA weld pool oscillation. Weld. J. 69, 289–293.
Xiao, Y., Den Ouden, G., 1993. Weld pool oscillation during GTA welding of mild steel. Weld. J. 72, 428–434.
YOO, C.D., Richardson, R.W., 1993. An experimental study on sensitvity and signal characteristics of welds pool oscillation. Trans. Jpn. Weld. Soc. 24, 54–62.
Zacksenhouse, M., Hardt, D., 1983. Weld pool impedance identification for size measurement and control. J. Dyn. Syst. Meas. Control 105, 179–184.
Zhang, K., Zhang, Y., Chen, J., Wu, S., 2017. Observation and analysis of three-dimensional weld pool oscillation dynamic behaviors. Weld. J. 96, 143–153.
Zhang, W., Liu, Y., Wang, X., Zhang, Y.M., 2012. Chracterization of three-dimensional weld Pool surface in GTAW. Weld. J. 91, 195–203.
Zhang, Y.M., Song, H.S., Saeed, G., 2006. Observation of a dynamic specular weld pool surface. Meas. Sci. Technol. 17, 9–12.